Synthesis mechanism of cuprous oxide nanoparticles by atmospheric-pressure plasma electrolysis

Jiandi Liu, Naoki Shirai, and Koichi Sasaki

Division of Applied Quantum Science and Engineering, Hokkaido University, Kita 13, Nishi 8, Kita-ku, Sapporo 060-8628, Japan

E-mail: ljd920911@eis.hokudai.ac.jp and nshirai@qe.eng.hokudai.ac.jp

Abstract. The synthesis mechanism of cuprous oxide (Cu_2O) nanoparticles by atmospheric-pressure plasma electrolysis was investigated experimentally. In the plasma electrolysis system, a helium plasma in contact with an NaCl electrolyte was used as the cathode, while a copper plate which was partly immersed into the electrolyte was used as the counter electrode. X-ray powder diffraction, field-emission scanning electron microscopy, and transmission electron microscopy were used for characterizing the synthesized products. The results indicate that the Cl^- concentration and the pH value of the electrolyte dominate the synthesis of Cu_2O nanoparticles. The reaction between $CuCl_2^-$ produced via the anodic dissolution of Cu and OH^- produced by plasma irradiation is responsible for the formation of Cu_2O. The comparison between the plasma and conventional electrolysis has also been carried out, since the anodic dissolution of the Cu plate and the production of OH^- are also available in the conventional electrolysis. As a result, we also observed the synthesis of Cu_2O nanoparticles by the conventional electrolysis. However, we observed the differences between the plasma and conventional electrolysis in the synthesis rate, the minimum NaCl concentration, and the size and the shape of synthesized nanoparticles.

Submitted to: *J. Phys. D: Appl. Phys.*

1. Introduction

Cu_2O is a widely studied semiconductor material with a narrow band-gap energy of 2.17 eV [1–3]. Because of its unique optical, electronic, and magnetic properties, Cu_2O is a promising material which has been applied in many areas such as catalysis [4–11], Li-ion battery [12–14], gas sensing [15, 16], magnetic storage [17], solar cells [18, 19, 31], and water splitting [21]. Recently, nanoparticles have drawn much attention because of its unique properties and potential applications. In order to synthesize Cu_2O nanoparticles with specific sizes and morphologies, various methods have been developed including chemical precipitate methods [22], hydrothermal treatments [23], sonochemical methods [24], and γ-ray irradiation [25]. However, it is still urgent to find a simple, low-cost synthesis method.

The plasma-liquid interaction has recently attracted much attention in the fields of water treatment, material processing, and biomedicine [26–32]. When a plasma contacts with a liquid, the plasma-liquid interface appears and generates a great amount of highly reactive species. These reactive species can be transported into the bulk liquid, and they lead to further physical and chemical reactions in the solution. Consequently, the plasma-liquid interface as well as the bulk liquid becomes the reaction zone for many specific physical and chemical processes. Numerous researches report that this reaction zone can be used for synthesizing novel nanomaterials such as noble metals [33–39], magnetic materials [40–43], and alloys [44–46] in suitable conditions.

The plasma electrolysis is a novel technology based on the plasma-liquid interaction. The system of the plasma electrolysis is similar to the conventional electrolysis except that a solid electrode is replaced with a gaseous plasma. The use of the gaseous plasma instead of the solid electrode benefits from the plasma-liquid interactions and turns the conventional electrolysis into the plasma electrolysis. Because the plasma electrolysis is composed of a plasma and a liquid, both of the plasma and liquid parameters can influence the properties of final products.

In previous works, we have used atmospheric-pressure plasma electrolysis for synthesizing Cu_2O nanoparticles and investigated the effect of additive surfactants such as glucose, ascorbic acid, and cetyltrimethylammonium bromide (CTAB) [47–49]. These works focused the influence of the surfactants, and the synthesis route of Cu_2O is still unknown. We originally expected the reduction effects in the plasma electrolysis, which are considered to be driven by solvated electrons and/or atomic hydrogen, since avoiding the oxidation from Cu^+ to Cu^{2+} is the key for the synthesis of Cu_2O. However, we observed that the production of Cu_2O occurred in the vicinity of the anode plate even though the plasma was used as the cathode in the electrolysis system. In this work, we have investigated the effects of several parameters in the plasma electrolysis to understand the mechanism of the Cu_2O synthesis. As a result, we have found that the principal function of the plasma is not avoiding the oxidation of Cu^+ with the help of solvated electrons and atomic hydrogen. We have observed that the synthesis of Cu_2O is possible even by the conventional electrolysis. However, we have found the differences between the plasma and conventional electrolysis in the synthesis rate, the minimum concentration of the solute (NaCl), and the size and shape of synthesized nanoparticles.

2. Experimental procedure

Figure 1 shows the schematic diagram of the experimental apparatus for the sample preparation. Sodium chloride (NaCl) was dissolved into pure water to prepare the electrolyte with concentrations of 0.25, 0.5 and 1.0 M. The volume of the electrolyte was 50 mL.These concentrations resulted in the electrical conductivities of 23.75, 46 and 87 mS/m. A pre-polished copper plate (99.8%), which was partly immersed into the electrolyte, was used as the anode. The cathode was an atmospheric-pressure helium plasma which was generated between a brass tube (0.5 and 0.8 mm in inner and outer

diameters, respectively) and the electrolyte surface. During the discharge, one plasma spot which had a ring-like structure was observed on the electrolyte surface and changed negligible in all experiments The tip of the brass tube was placed at a distance of 3 mm from the electrolyte surface .This distance was kept during discharge when the electrolyte was 50 mL. Helium was fed toward the electrolyte surface from the tube in air. The gas flow rate was maintained at 200 sccm which was controlled using a mass flow controller. A direct-current power supply (Matsusada HAR-5P120) was used for producing a glow discharge along the helium flow. The voltage between the brass tube and the electrolyte was measured using a high voltage probe (Tektronix P6015A). In order to create a stable plasma discharge, the discharge current was kept at 20 mA. And the duration of the discharge or the electrolysis reaction was 20 min. It is noted that the changes in the voltage and the current were negligible during the electrolysis experiment. After the discharge, the suspension which included synthesized nanoparticles was concentrated by the centrifugation (5500 rpm, 5min), and nanoparticles were washed with purified water and ethyl alcohol for three times. After that, the sample was dried in an oven at 50 °C for 10 h for the characterization. We employed powder X-ray diffraction (XRD, Rigaku SmartLab 9 kW), field emission scanning electron microscopy (FESEM, JEOL JSM-7001FA), and transmission electron microscopy (TEM, JEOL JEM-2010 operated at 200 kV) for characterizing synthesized nanoparticles.

3. Synthesis of Cu_2O nanoparticles by plasma electrolysis

3.1. Effect of NaCl concentration

Several concentrations of NaCl, ranging between 0.25 and 1.0 M, were used for examining the effect of the Cl^- concentration on the synthesis of Cu_2O nanoparticles. Figure 2 shows the XRD patterns of the products synthesized at three NaCl concentrations. It is obvious that the major diffraction peaks of these samples coincide with the peaks of Cu_2O listed in the JCPDS database (No. 05-0667). On the other hand, the peaks corresponding to $Cu_2(OH)_3Cl$ were also found in all the samples synthesized at different NaCl concentrations. In addition, the peaks of by-product CuO were observed for the sample synthesized at an NaCl concentration of 0.25 M. This result indicates that the formations of Cu_2O and by-product CuO are related with the NaCl concentration. A higher concentration of NaCl solution is more suitable for the formation of Cu_2O.

Figure 3 shows FESEM pictures of nanoparticles synthesized at three NaCl concentrations. It is easy to understand that the NaCl concentration had strong effect on the size of nanoparticles. The nanoparticles were composed of octahedrons, fibers, and small flakes with irregular sizes in all the cases. In the case of the 1.0 M NaCl solution, the sizes of octahedrons were larger than 1 μm, and the apexes of octahedrons were corroded as shown in Fig. 3(a). In the case of the 0.5 M NaCl solution, octahedrons with the size of $\sim$ 500 nm were observed, and they had relatively sharp apexes. In the case of the 0.25 M NaCl solution, large-size octahedrons disappeared and the relative

abundance of fiber structures increased, as shown in Fig. 3(c).

The details of the microstructure of nanoparticles synthesized at an NaCl concentration of 1.0 M were further investigated by TEM. Figure 4(a) demonstrates that the sample was composed of octahedrons and fiber structures, which is the same result as the FESEM pictures shown in Fig. 3(a). Figures 4(b) and 4(c) show the selected-area electron diffraction (SAED) patterns. The selected areas are indicated in Fig. 4(a). Figure 4(b) shows the SAED pattern which is taken from the edge of an octahedron structure. According to the SAED pattern, the lattice fringes with interlayer spacings of 0.246 and 0.135 nm can be attributed to the (111) and (310) facets of Cu_2O, respectively. The SAED pattern which was taken from the fiber structure is shown in Fig. 4(c). The SAED pattern shows the interlayer spacings of 0.303, 0.193, and 0.252 nm, which can be attributed to the (200), (222) and (103) facets of $Cu_2(OH)_3Cl$, respectively.

3.2. Effect of dissolved oxygen

It is well known that oxygen can dissolve into solutions. In general, dissolved oxygen (DO) affects chemical reactions in the solution. For example, Yamazaki and coworkers have reported that the DO concentration is a key parameter in the synthesis of magnetite nanoparticle by glow-discharge electrolysis [43]. The concentration of DO significantly determines the kind of the final product, nonmagnetic hematite (Fe_2O_3) nanoparticles or ferromagnetic magnetite (Fe_3O_4) nanoparticles.

As described in Sec. 3.1, the peaks corresponding to CuO were found in the XRD pattern only for the sample synthesized at an NaCl concentration of 0.25 M. It is noted here that the DO concentration is affected by the salinity. This suggests the possibility that the NaCl concentration works as an indirect parameter to control the DO concentration, and the direct parameter which dominates the synthesis of Cu_2O is the DO concentration. Hence, we examined the effect of the DO concentration on the synthesis characteristics with keeping the NaCl concentration at 0.25 M.

The DO concentration was varied by changing the duration of the nitrogen bubbling. The DO concentration was measured using a commercial DO meter. The DO concentration of the 0.25 M NaCl solution was 7.9 mg/L when the nitrogen bubbling was not adopted. The DO concentrations after the nitrogen bubbling for 1, 2.5, 5, and 10 min were 6.4, 5.2, 3.7 and 1.9 mg/L, respectively. It is noted that the recovery of the DO concentration was slow and it changed from 1.0 to 3.1 mg/L after the one-night aging. The XRD patterns of the samples synthesized at several DO concentrations are shown in Fig. 5. As shown in the XRD patterns, the strong peaks corresponding to Cu_2O and the weak peaks corresponding to CuO were observed in all the samples, and it was difficult to find the difference in the products synthesized at different DO concentrations. Therefore, it is suggested that the DO concentration has negligible effect on the synthesis of Cu_2O nanoparticles.

3.3. Effect of pH value

In general, the pH value of the solution is a non-negligible factor in most researches using aqueous solutions as well as the plasma electrolysis. The pH value of the 0.5 M NaCl solution with no additives was 5.8. The pH values of the 0.5 M NaCl solutions before starting the electrolysis were controlled between 10.5 and 3.2 by adding various amounts of hydrochloric acid (HCl) or sodium carbonate (Na_2CO_3). The XRD patterns of the products synthesized at several pH values are shown in Fig. 6. We observed that the XRD pattern of the sample synthesized at a pH value of 3.2 was significantly different from those synthesized at other pH values. In the cases of the alkaline conditions with pH values of 10.5 and 8.0, the products are the mixture of Cu_2O and $Cu_2(OH)_3Cl$. The sample synthesized at a weak acid condition with a pH value of 5.8 was similar to those synthesized at alkaline conditions. In contrast, in the sample synthesized at a strong acid condition with a pH value of 3.2, only the peaks of $Cu_2(OH)_3Cl$ were observed and the peaks of Cu_2O disappeared. This result demonstrates that the pH value of the electrolyte has significant influence on the synthesis of Cu_2O nanoparticles.

Even though the pH value before starting the electrolysis was controlled, it was varied during the electrolysis by the production of OH^- from the region of the electrolyte in contact with the plasma cathode [50]. The pH values after the electrolysis were 10.7, 10.3, 10.0 and 5.7 when the original values were 10.5, 8.0, 5.8 and 3.2, respectively. The pH value was still lower than 6 after the electrolysis only when the original pH value was 3.2, and as shown in Fig. 6, Cu_2O nanoparticles were not synthesized only in this case. Note that these pH values were volume-averaged ones in the reactor.

In order to observe the variation of the pH value visually during the discharge, a pH indicator named bromothymol blue (BTB) was admixed into the electrolyte. The BTB-admixed electrolyte is yellow in the acid condition ($pH \leq 6$), but the color is blue when the pH value is higher than 7.6. Figure 7 shows the temporal variation of the color of the BTB-admixed electrolyte, together with the pictures of the reactor with no BTB admixture at the same delay times after the initiation of the discharge. The pH value before the initiation of the discharge was 5.8 and the color of the electrolyte was yellow as shown in Fig. 7(a). At 30 s after the initiation of the discharge, we observed that the electrolyte just below the plasma cathode became alkaline, as shown in Fig. 7(c). This is due to the production of OH^-. The blue area expanded toward the Cu anode area. At the same time, we observed the production of yellow insoluble precipitates from the anode, as shown in Fig. 7(d). This insoluble precipitates were Cu_2O nanoparticles. The blue or alkaline area expanded to the most region of electrolyte at 2 min after the initiation of the discharge, as shown in Fig. 7(e). Meanwhile, the insoluble yellow precipitates diffused to the entire region of the electrolyte as shown in Fig. 7(f). This result indicates that an alkaline condition or a high concentration of OH^- around the anode Cu plate is an important factor for the synthesis of Cu_2O nanoparticles.

4. Synthesis mechanism of Cu_2O nanoparticles

On the basis of the aforementioned experimental results, we propose the synthesis mechanism of Cu_2O nanoparticles illustrated in Fig. 8. The synthesis mechanism has two steps. The first step is the production of $CuCl_2^-$ [51]. When the electrolysis is started, the Cu plate (the anode) releases Cu^+ ions via the anodic dissolution,

$$Cu^0 \rightarrow Cu^+ + e^-. \tag{1}$$

If the concentration of Cl^- (namely the concentration of NaCl) is sufficiently high, Cu^+ combines with Cl^- immediately after the production to form $CuCl_2^-$,

$$Cu^+ + 2Cl^- \rightarrow CuCl_2^-. \tag{2}$$

It is noted that the oxidation of Cu^+ to Cu^{2+} is avoided by this reaction. Other possibilities for the production process of $CuCl_2^-$ are the direct production from the electrode via

$$Cu^0 + 2Cl^- \rightarrow CuCl_2^- \tag{3}$$

and the partial chloridation

$$Cu^0 + Cl^- \rightarrow CuCl + e^- \tag{4}$$

followed by

$$CuCl + Cl^- \rightarrow CuCl_2^-. \tag{5}$$

A high Cl^- concentration is important in all the production processes of $CuCl_2^-$.

The second step is the reaction between $CuCl_2^-$ and OH^-. OH^- is generated under the irradiation point of the plasma, as shown in Fig. 7(c). The production of OH^- could be owing to the reaction between OH radicals and solvated electrons at the plasma-liquid interface. OH^- ions are transported toward the Cu anode. When OH^- reaches the anode, Cu_2O is formed via the following reaction,

$$2CuCl_2^- + 2OH^- \rightarrow Cu_2O + H_2O + 4Cl^-. \tag{6}$$

The importance of this reaction is confirmed by the experimental results shown in Figs. 7(e) and 7(f), where we observed the production of Cu_2O nanoparticles when OH^- (or the blue region) arrived at the anode. If the OH^- concentration is insufficient, Cu^+ is oxidized to Cu^{2+} via

$$CuCl_2^- \rightarrow Cu^{2+} + 2Cl^- + e^-. \tag{7}$$

The formation of Cu^{2+} results in the productions of $Cu_2(OH)_3Cl$ and CuO via

$$2Cu^{2+} + 3OH^- + Cl^- \rightarrow Cu_2(OH)_3Cl \tag{8}$$

and

$$Cu^{2+} + OH^- \rightarrow CuO + H_2O, \tag{9}$$

respectively. These are the mechanism for the enhancement of the productions of $Cu_2(OH)_3Cl$ and CuO at a low pH value (Fig. 6).

As described above, there are three important factors for the efficient synthesis of Cu_2O nanoparticles: 1) the high concentration of Cl^-, 2) the production of a large amount of OH^-, and 3) the efficient transport of OH^- toward the anode. We tested the synthesis of Cu_2O nanoparticles by using $NaNO_3$ solutions with concentrations of 0.25, 0.5 and 1.0 M. As a result, we did not observe Cu_2O nanoparticles and the products were occupied by CuO. This result suggests that $CuCl_2^-$ is the particular intermediate for the synthesis of Cu_2O.

5. Synthesis of Cu_2O nanoparticles by conventional electrolysis

It is well known that OH^- is produced on the cathode via

$$2H_2O + 2e^- \rightarrow H_2 + 2OH^- \tag{10}$$

in the conventional electrolysis. Therefore, according to the aforementioned mechanism, the plasma electrolysis is not the unique method for the synthesis of Cu_2O nanoparticles. Figure 9 shows the pictures of the reactor when the plasma cathode was replaced with a carbon rod which was immersed into the NaCl solution with the admixture of BTB. The NaCl concentration was 0.5 M. As shown in the figure, we observed the synthesis of Cu_2O nanoparticles from the Cu anode. However, we needed a much longer time to observe the production of Cu_2O. This may be due to the less efficient production and transport of OH^- toward the anode.

Figure 10 shows the XRD patterns of the products synthesized by conventional electrolysis at three NaCl concentrations between 0.25 and 1.0 M. In the case of the 1.0 M NaCl solution, we observed only the peaks corresponding to Cu_2O. The peaks corresponding to $Cu_2(OH)_3Cl$ and CuO appeared in the case of the 0.5 M NaCl solution. In addition, at an NaCl concentration of 0.25 M, the peaks corresponding to Cu_2O disappeared, and the product was occupied by $Cu_2(OH)_3Cl$ and CuO.

The FESEM images of nanoparticles synthesized by the conventional electrolysis at three NaCl concentrations are shown in Fig. 11. It is obvious that the NaCl concentration affects the size and the shape of synthesized nanoparticles. In the case of the 1.0 M NaCl solution, nanoparticles were composed of octahedrons, fibers, and small flakes. The size of octahedrons was smaller than 1 μm, and octahedrons had sharp apexes, as shown in Fig. 11(a). The morphologies of nanoparticles synthesized at NaCl concentrations of 0.5 and 0.25 M were similar. Octahedrons were not observed, and the products were occupied by flakes and fibers. The flower shape structures, which were probably aggregated fibers, were also observed.

The samples synthesized at NaCl concentrations of 1.0 and 0.5 M were analyzed by TEM. Figure 12(a) demonstrates that the sample synthesized at the 1.0 M NaCl solution was composed of octahedrons and fiber structures. Figure 12(b) shows the SAED pattern which was taken from the edge of an octahedron. The SAED pattern shows that the octahedron is Cu_2O having the (110), (111), and (211) facets with interlayer spacings of 0.302, 0.246, and 0.174 nm, respectively. Figure 12(c) shows the

detailed image of the fiber structure synthesized at an NaCl concentration of 0.5 M. The SAED pattern of the fiber structure is shown in Fig. 12(d). The diffraction rings centered at the transmission spot can be indexed as (113) and (411) with interlayer spacings of 0.237 and 0.142 nm, respectively, indicating that the fiber structure is the polycrystal of $Cu_2(OH)_3Cl$.

6. Comparison between Cu_2O nanoparticles synthesized by plasma and conventional electrolysis

We find three differences between the plasma and conventional electrolysis for the synthesis of Cu_2O nanoparticles. The first difference is the synthesis rate of Cu_2O, especially at a short ($\leq$ 2 min) delay time after the initiation of the electrolysis. The much higher synthesis rate of the plasma electrolysis than the conventional electrolysis is obtained by the much efficient transport of OH^- toward the anode. The efficient transport of OH^- in the plasma electrolysis is due to the induction of a liquid flow by the plasma-liquid interaction [52].

The second difference is the minimum NaCl concentration at which Cu_2O nanoparticles can be synthesized. In the conventional electrolysis, we did not observe Cu_2O at an NaCl concentration of 0.25 M, as shown in Fig. 10(c), whereas as shown in Fig. 2(c), Cu_2O was produced at the same NaCl concentration in the plasma electrolysis. This difference could be related with the reduction ability in the plasma electrolysis. It is reported that solvated electrons and atomic hydrogen are produced by the plasma-liquid interaction, and they can work as reduction agents in the liquid in the plasma electrolysis [53]. However, it is impossible to expect the transports of solvated electrons and atomic hydrogen to the anode, since they are short-lived species. At the moment, we cannot point out the concrete reduction agents which work around the anode area, if the synthesis of Cu_2O at a low NaCl concentration is owing to the reduction ability of the plasma electrolysis.

The third difference is found in size and the shape of synthesized nanoparticles. As shown in Figs. 3 and 11, the plasma electrolysis synthesized larger-size octahedron Cu_2O than the conventional electrolysis. The fractional abundances of fibers and flakes were greater in the conventional electrolysis at the same NaCl concentration. In addition, the crystallinity of the fiber structures were completely different, as shown in Figs. 4 and 12. The mechanism which causes the difference in the morphology and the crystallinity of synthesized nanoparticles is left as an issue in the future work.

7. Conclusions

We have investigated the synthesis mechanism of Cu_2O nanoparticles by the atmospheric-pressure plasma electrolysis in the NaCl solution. The results indicate that the Cl^- concentration and the pH value of the electrolyte dominate the synthesis of Cu_2O nanoparticles. Cu^+ ions which are released via the anodic dissolution of Cu

combine with Cl^- to form $CuCl_2^-$ at the surface of the Cu plate. Meanwhile, OH^- ions produced by the plasma irradiation are soon transported toward the Cu anode. When OH^- ions reach the surface of the Cu plate, the formation of Cu_2O occurs by the reaction between $CuCl_2^-$ and OH^-. A high NaCl concentration, the efficient generation of OH^-, and the fast transport of OH^- are the important factors for the efficient formation of Cu_2O. The concentration of dissolved oxygen does not affect the synthesis of Cu_2O. The results also indicate that the plasma electrolysis is not a unique method to synthesize Cu_2O nanoparticles. Cu_2O nanoparticles can also be formed by the conventional electrolysis. The differences between the plasma and conventional electrolysis are the synthesis rate, the minimum NaCl concentration, and the size and the shape of synthesized nanoparticles.

Acknowledgments

JL is grateful to China Scholarship Council (CSC) for the support to study in Hokkaido University. This work was supported by JSPS KAKENHI Grant Nos. 16H02121, 18K03596, and 20H00135.

References

[1] Shen M Y, Yokouchi T, Koyama S, and Goto T 1997 *Phys. Rev .B* **56** 13066
[2] Ghijsen J, Tjeng L H, van Elp J, Eskes H, Westerink J, Sawatzky G A, and Czyzyk M T 1998 *Phys. Rev. B* **38** 11322
[3] Lu C, Qi L, Yang J, Wang X, Zhang D, Xie J, and Ma J 2005 *Adv. Mater.* **17** 2562
[4] Barreca D, Fornasiero P, Gasparotto A, Gombac V, Maccato C, Montini T, Tondello E 2009 *ChemSusChem* **2** 230
[5] Huang L, Peng F, Yu H, and Wang H J 2009 *Solid State Sci.* **11** 129
[6] Zhang Y, Deng B, Zhang T R, Gao D M, and Xu A W 2010 *J. Phys. Chem. C* **114** 5073
[7] Xu H L, Wang W Z, and Zhu W 2006 *J. Phys. Chem. B* **110** 13829
[8] Shoeib M A, Abdelsalam O E, Khafagi M G, and Hammam R E 2012 *Adv. Powder Technol.* **23** 298
[9] Ho J Y and Huang M H 2009 *J. Phys. Chem. C* **113** 14159
[10] Ji R, Sun W D, and Chu Y 2013 *ChemPhysChem* **14** 3971
[11] Zheng H Y, Li Q, Yang C M, Lin H, Nie M, Qin L Z, and Li Y 2015 *RSC Adv.* **5** 59349
[12] Park J C, Kim J, Kwon H, and Song H 2009 *Adv. Mater.* **21** 803
[13] Hara M, Kondo T, Komoda M, Ikeda S, Shinohara K, Tanaka A, Kondo J N, and Domen K 1998 *Chem. Commun.* **3** 357
[14] Ikeda S, Takata T, Kondo T, Hitoki G, Hara M, Kondo J N, Domen K, Hosono H, Kawazoe H, and Tanaka A 1998 *Chem. Commun.* **20** 2185
[15] Deng S, Tjoa V, Fan H M, Tan H R, Sayle D C, Olivo M, Mhaisalkar S, Wei J, and Sow C H 2012 *J. Am. Chem. Soc.* **134** 4905
[16] Zhang J T, Liu J F, Peng Q, Wang X, and Li Y D 2006 *Chem. Mater.* **18** 867
[17] Li X D, Gao H S, Murphy C J, and Gou L F 2004 *Nano Lett.* **4** 1903
[18] Cui J B and Gibson U J 2010 *J. Phys. Chem. C* **114** 6408
[19] Zhao W Y, Fu W Y, Yang H B, Tian C J, Ge R X, Wang C J, Liu Z L, Zhang Y Y, Li M H, and Li Y X 2010 *Appl. Surf. Sci.* **256** 2269
[20] Wang W Z, Wang G H, Wang X S, Zhan Y J, Liu Y K, and Zheng C L 2002 *Adv. Mater.* **14** 67

[21] de Jongh P E, Vanmaekelbergh D, and Kelly J J 1999 *Chem. Commun.* **12** 1069
[22] Gou L F and Murphy C J 2003 *Nano Lett.* **3** 231
[23] Huang W C, Lyu L M, Yang Y C, and Huang M H 2012 *J. Am. Chem. Soc.* **134** 1261
[24] Sun D D, Du Y, Tian X Y, Li Z F, Chen Z T, and Zhu C F 2014 *Mater. Res. Bull.* **60** 704
[25] Liu W J, Chen G H, He G H, and Zhang W 2011 *J. Nanopart. Res.* **13** 2705
[26] Bruggeman P and Leys C 2009 *J. Phys. D: Appl. Phys.* **42** 053001
[27] Locke B R, Sato M, Sunka P, Hoffman M R, and Chang J S 2006 *Ind. Eng. Chem. Res.* **45** 882
[28] Vanraes P, and Bogaerts A 2018 *Appl. Phys. Rev.* **5** 031103
[29] Foster J E 2017 *Phys. Plasma* **24** 055501
[30] Foster J E, Mujovic S, Groele J and Blankson I M 2018 *J. Phys. D: Appl. Phys.* **51** 293001
[31] Wang C, Qu G Z, Wang T C, Deng F and Liang D L 2018 *Chem. Eng. J* **349** 159
[32] Bruggeman P et al 2016 *Plasma Sources Sci. Technol.* **25** 053002
[33] Chen Q, Li J, and Li Y 2015 *J. Phys. D: Appl. Phys.* **48** 424005
[34] Saito G and Akiyama T 2015 *J. Nanomater.* **2015** 123696.
[35] Huang X, Li Y, and Zhong X 2014 *Nanoscale Res. Lett.* **9** 1
[36] Huang X Z, Zhong X, Lu Y, Li Y S, Rider A E, Furman S A, and Ostrikov K 2013 *Nanotechnol.* **24** 095604
[37] Wang R, Zuo S, Wu D, Zhang J, Zhu W, Becker K H, and Fang J 2015 *Plasma Process. Polym.* **12** 380
[38] Meiss S A, Rohnke M, Kienle L, Zein El Abedin S, Endres F, and Janek J 2007 *ChemPhysChem* **8** 50
[39] Höfft O and Endres F 2011 *Phys. Chem. Chem. Phys.* **13** 13472
[40] Toriyabe Y, Watanabe S, Yatsu S, Shibayama T, and Mizuno T 2007 *Appl. Phys. Lett.* **91** 041501
[41] Saito G, Hosokai S, Tsubota M, and Akiyama T 2011 *Plasma Chem. Plasma Process.* **31** 719
[42] Shirai N, Yoshida T, Uchida S, and Tochikubo F 2017 *Jpn. J. Appl. Phys.* **56** 076201
[43] Yamazaki Y, Shirai N, Nakagawa Y, Uchida S, and Tochikubo F 2018 *Jpn. J. Appl. Phys.* **57** 096201
[44] Tokushige M, Yamanaka T, Matsuura A, Nishikiori T, and Ito Y 2009 *IEEE Tran. Plasma Sci.* **37** 1156
[45] Tokushige M, Nishikiori T, Lafouresse M, Michioka C, Yoshimura K, Fukunaka Y, and Ito Y 2010 *Electrochim. Acta* **55** 8154
[46] Pootawang P, Saito N, Takai O, and Lee S Y 2012 *Nanotechnol.* **23** 395602
[47] Liu J D, He B B, Chen Q, Liu H, Li J S, Xiong Q, Zhang X H, Yang S Z, Yue G H, and Liu Q H 2016 *Electrochimica Acta* **222** 1677
[48] Liu J D, He B B, Wang X, Chen Q and Yue G H 2019 *Eur. Phys. J. D* **73** 11
[49] Liu J D, Chen Q, Li J S, Xiong Q, Yue G H, Zhang X H, Yang S Z and Liu Q H 2016 *J. Phys. D: Appl. Phys.* **49** 275201
[50] Shirai N, Uchida S, and Tochikubo F 2014 *Jpn. J. Appl. Phys.* **53** 046202
[51] Kear G, Barker B D, and Walsh F C 2004 *Corros. Sci.* **46** 109
[52] Rumbach P, Griggs N, Sankaran R M and David B G 2014 *IEEE Trans Plasma Sci* **42** 2610
[53] Rumbach P, Bartels D M, Sankaran R M and David B G 2015 *Nat. Commun.* **6** 7248

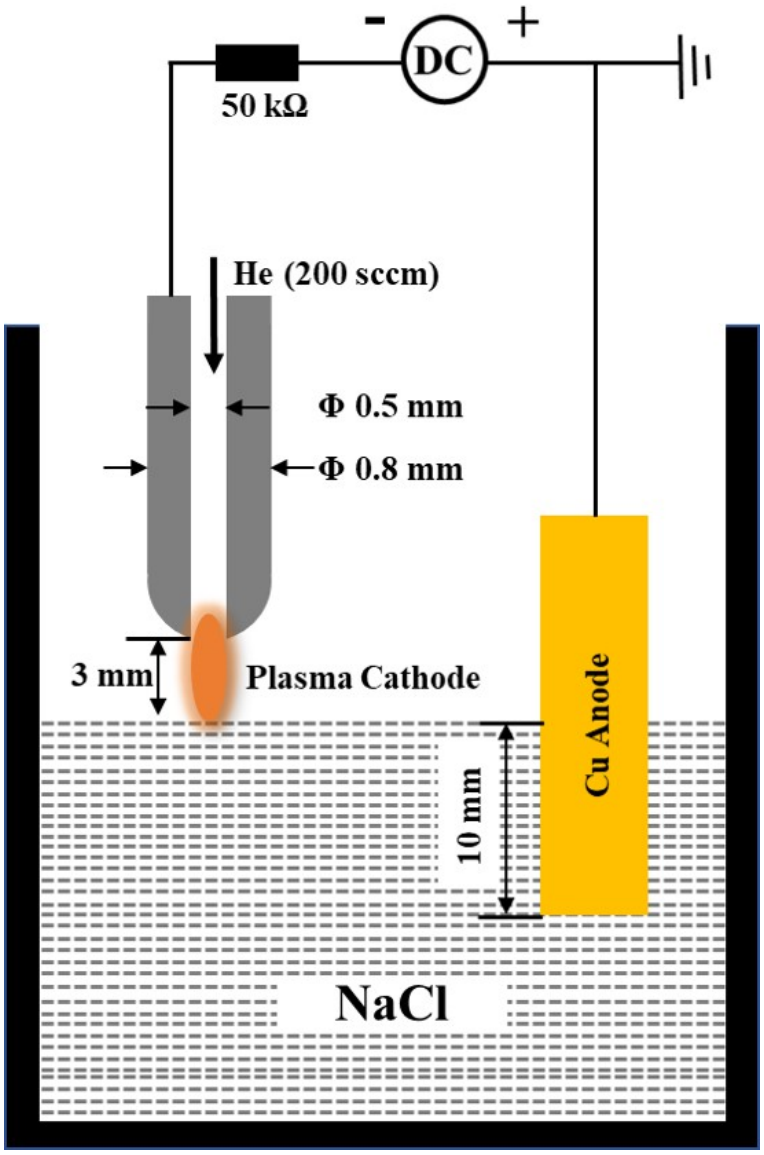

Figure 1. Schematic diagram of the experimental apparatus.

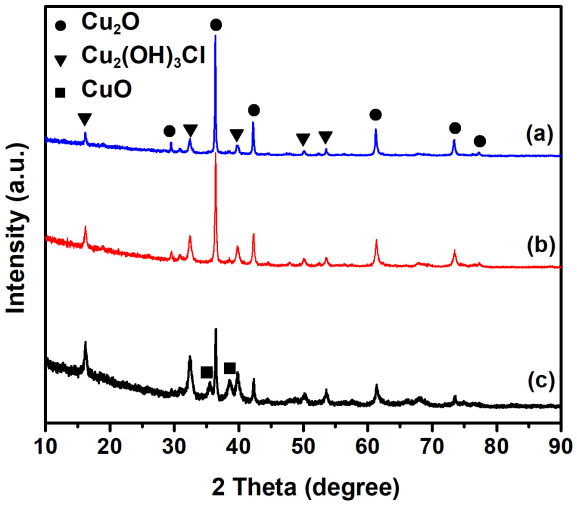

Figure 2. XRD patterns of nanoparticles synthesized at NaCl concentrations of (a) 1.0, (b) 0.5, and (c) 0.25 M.

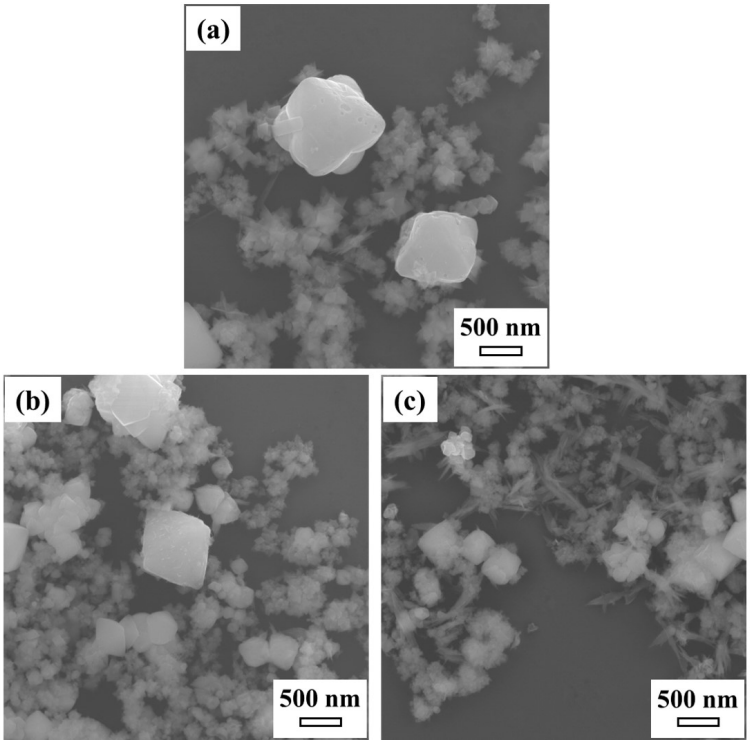

Figure 3. FESEM images of nanoparticles synthesized at NaCl concentrations of (a) 1.0, (b) 0.5, and (c) 0.25 M.

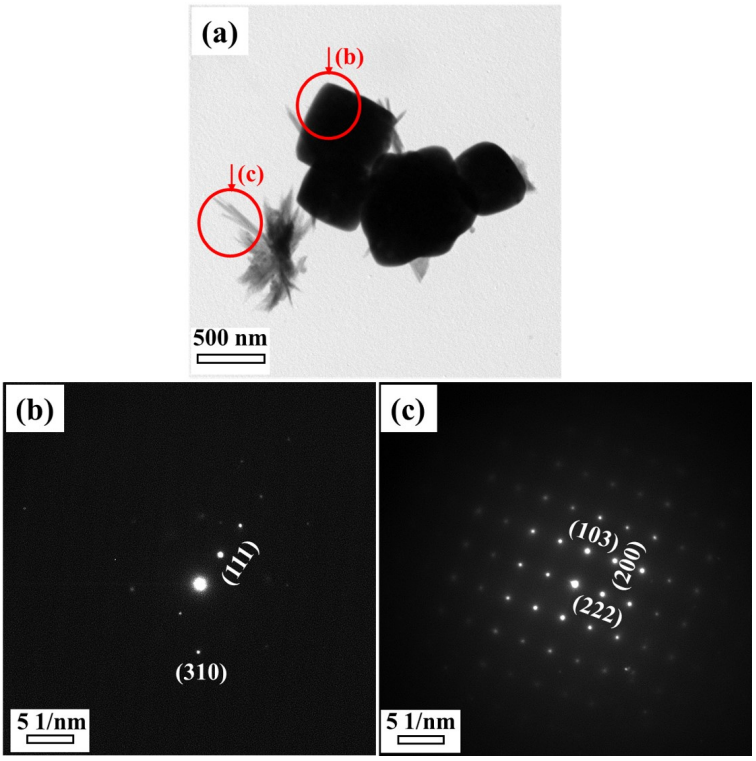

Figure 4. (a) TEM image of nanoparticles synthesized at an NaCl concentration of 1.0 M. (b) and (c) are SAED patterns of the regions indicates in (a) by circles.

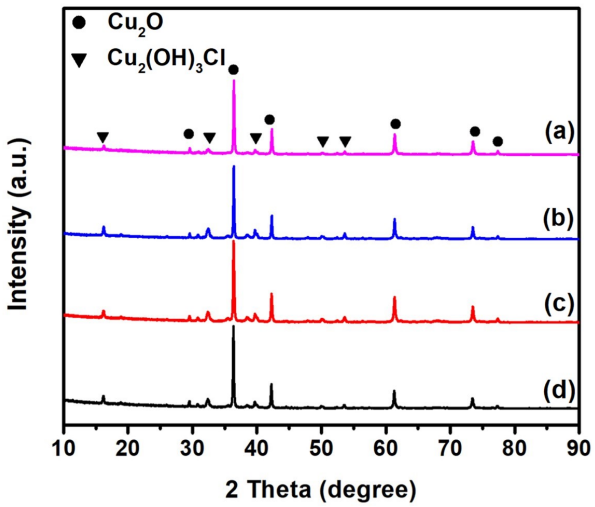

Figure 5. XRD patterns of nanoparticles synthesized at DO concentrations of (a) 6.4, (b) 5.2, (c) 3.7, and (d) 1.9 mg/L. The NaCl concentration was 0.25 M.

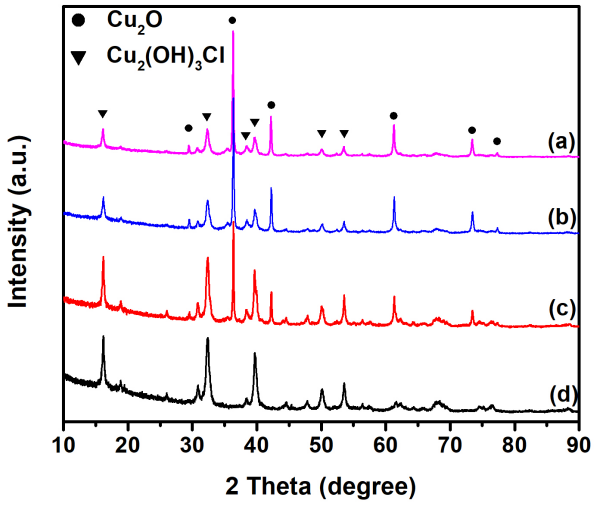

Figure 6. XRD patterns of nanoparticles synthesized in 0.5 M NaCl solutions with pH values of (a) 10.5, (b) 8.0, (c) 5.8, and (d) 3.2. The NaCl concentration was 0.5 M.

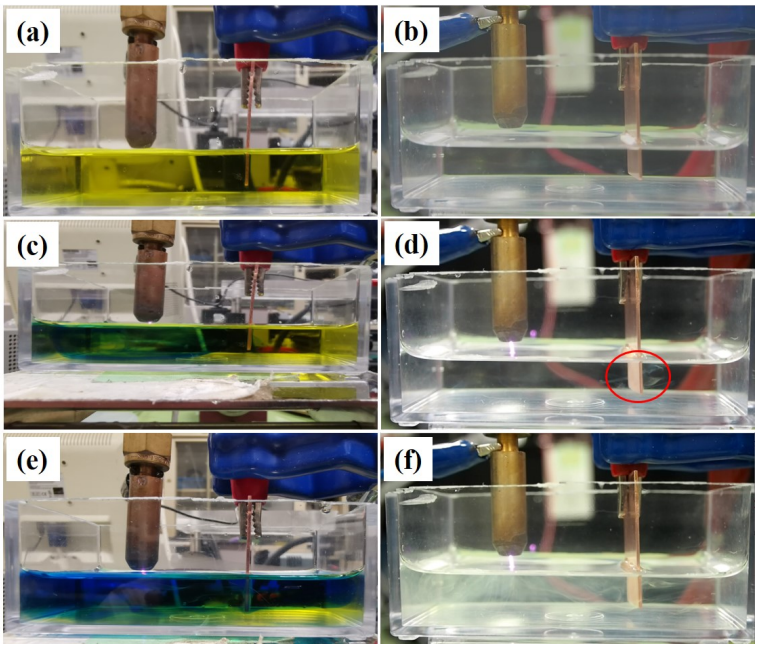

Figure 7. Photographs of reactors with ((a), (c), and (e)) and without ((b), (d), and (f)) the admixture of BTB. (a) and (b): before the discharge, (c) and (d): 30 s after the initiation of the discharge, and (e) and (f): at 2 min after the initiation of the discharge.

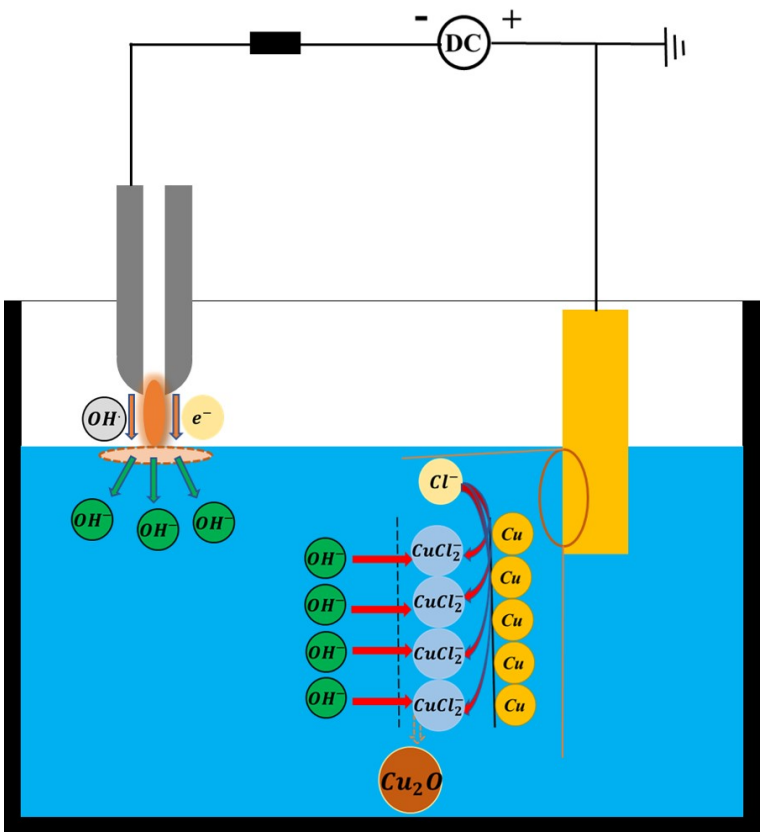

Figure 8. Schematic of possible synthesis mechanism of Cu_2O nanoparticles.

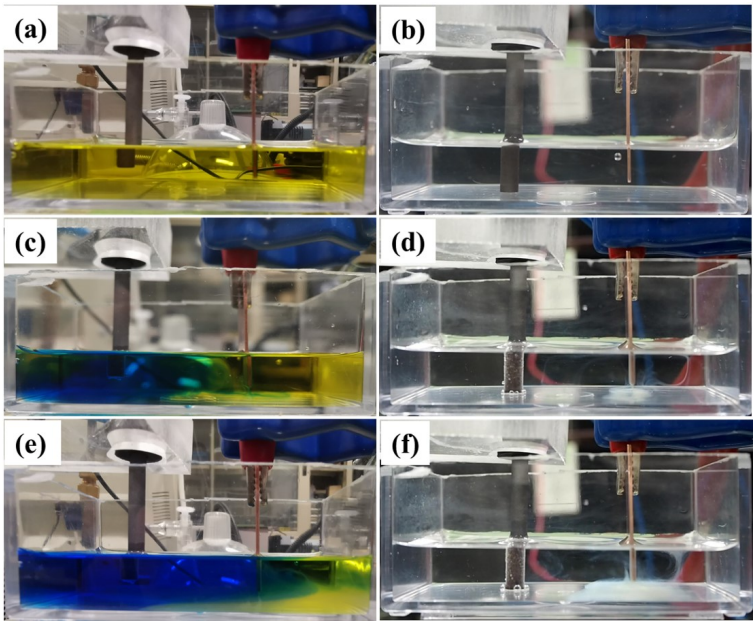

Figure 9. Photographs of reactors in conventional electrolysis with ((a), (c), and (e)) and without ((b), (d), and (f)) the admixture of BTB. (a) and (b): before the discharge, (c) and (d): 3 min after the initiation of the discharge, and (e) and (f) at 7 min after the initiation of the discharge.

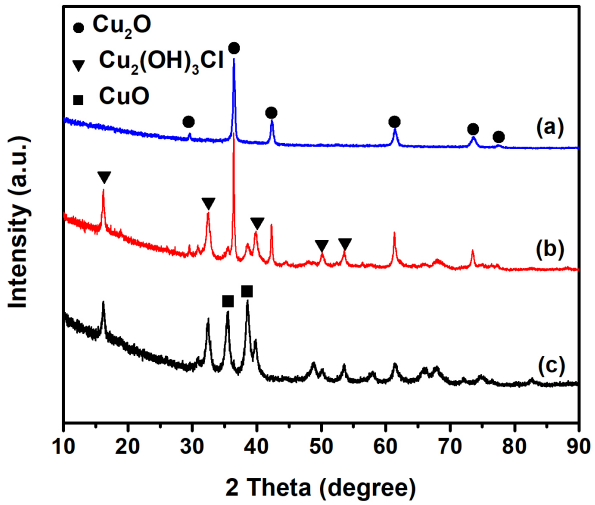

Figure 10. XRD patterns of nanoparticles synthesized by conventional electrolysis at NaCl concentrations of (a) 1.0, (b) 0.5, and (c) 0.25 M.

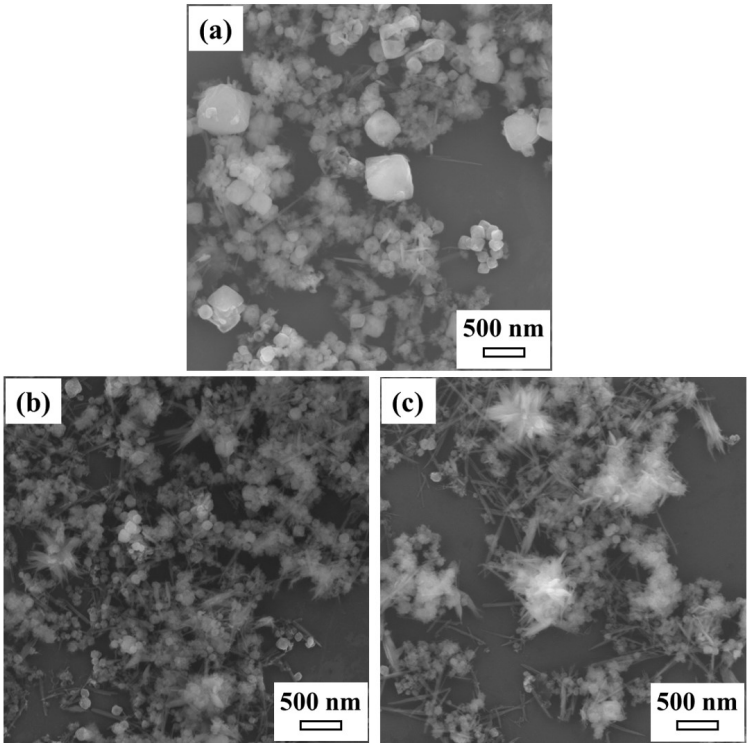

Figure 11. FESEM images of nanoparticles synthesized by conventional electrolysis at NaCl solutions of (a) 1.0, (b) 0.5, and (c) 0.25 M.

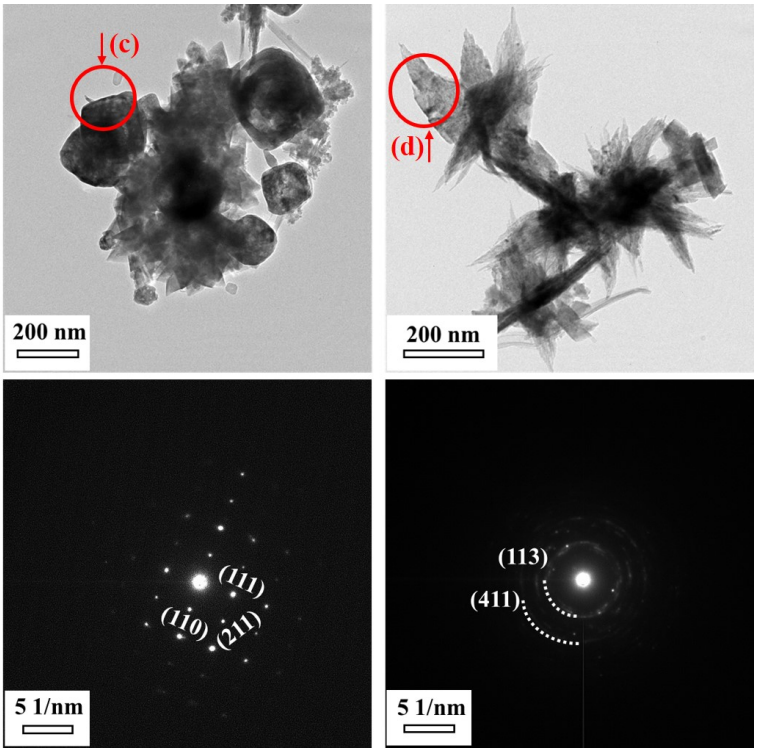

Figure 12. (a) and (c) show TEM images of nanoparticles synthesized by conventional electrolysis at NaCl concentrations of (a) 1.0 and (b) 0.5 M. (b) and (d) are SAED patterns of the regions indicated by circles in (a) and (c), respectively.